Tetrahedron 69 (2013) 1767–1777

Contents lists available at SciVerse ScienceDirect

Tetrahedron

journal homepage: www.elsevier.com/locate/tet

ESIPT inspired fluorescent 2-(4-benzo[*d*]oxazol-2-yl)naphtho[1,2-*d*]oxazol-2-yl)phenol: experimental and DFT based approach to photophysical properties

Kiran R. Phatangare [a,†], Vinod D. Gupta [a,b,†,‡], Abhinav B. Tathe [a,†], Vikas S. Padalkar [a,†], Vikas S. Patil [a,†], Ponnadurai Ramasami [b,*], Nagaiyan Sekar [a,*]

[a] *Tinctorial Chemistry Group, Department of Dyestuff Technology, Institute of Chemical Technology, N.P. Marg, Matunga, Mumbai 400 019, Maharashtra, India*
[b] *Computational Chemistry Group, Department of Chemistry, University of Mauritius, Réduit, Mauritius*

ARTICLE INFO

Article history:
Received 7 July 2012
Received in revised form 1 November 2012
Accepted 27 November 2012
Available online 6 December 2012

Keywords:
Benzoxazole
Naphthoxazole
ESIPT
Fluorescence
Solvatochromism
TD-DFT

ABSTRACT

ESIPT inspired fluorescent 2-(4-benzo[*d*]oxazol-2-yl)naphtho[1,2-*d*]oxazol-2-yl)phenol was synthesized from 1-amino-3-(1,3-benzoxazol-2-yl)naphthalen-2-ol. Photophysical behavior of the synthesized compound was studied using UV–visible and fluorescence spectroscopy in polar and non-polar solvents. The synthesized naphthoxazolyl benzoxazole is fluorescent and very sensitive to the micro-environment. It shows a single absorption and dual emission in non-polar solvents with large Stokes shift originating from Excited State Intramolecular Proton Transfer while in polar solvents only a single short wavelength emission is observed. Experimental absorption and emission wavelengths are in good agreement with those predicted using the Time-Dependent Density Functional Theory (TD-DFT) [B3LYP/6-31G(d)]. The largest wavelength difference between the experimental and computed absorption maxima was 16 nm (acetonitrile) and 7 nm (ethyl acetate, THF, and 1,4-dioxane) in the short and long wavelength regions, respectively. A largest difference of 25 nm was observed for the short wavelength emission in DMF and 22 nm for the longer wavelength emission in chloroform.

1. Introduction

Phototautomerization from Excited State Intramolecular Proton Transfer (ESIPT) is of prime importance in biological and chemical systems[1] and as a result, there have been experimental and theoretical interests.[2] Photoexcitation leads to a shift in electron density that facilitates proton migration from a donor atom, usually oxygen, to a nearby acceptor atom, either oxygen or nitrogen, culminating in ESIPT. In molecules with an oxygen donor, the ground state is the enol form (E), and the emissive excited state is the keto form (K*). The enol (E)–keto (K) phototautomerism takes place in many instances via five-,[3] six-,[4] or rarely seven-member[5] quasi transition state. Therefore, a dual fluorescence band could be observed as the absorption is from E → E* (E* is excited state enol form) and emission is from K* → K.

A large apparent Stokes red shift was observed in fluorescence due to the difference in energy between absorption by the original (enol) tautomer and emission from the resultant (keto) tautomer of the molecule.[6] Occurrence of this second red shifted emission makes such molecules interesting, and they find a wide range of applications as photochromic dyes,[7] laser dyes,[8] fluorescent probes,[9] sensors,[10] organic electroluminescence optical materials,[11] and photostabilizers[12] as well as in fluorescence recording techniques.[13]

The design, synthesis, and photophysical characterization of ESIPT organic molecules are of contemporary interest.[14] ESIPT is largely characterized by the energy level changes of E* → K*, and only small energy barrier or even barrierless is allowed. This could be justification for the fact the most ESIPT molecules are of small sizes. Molecules possessing acidic and/or basic groups are known to experience an enhancement of acidity and/or basicity upon excitation. Specifically, molecules having an acidic group and basic site hydrogen bonded in the ground state can undergo an ultrafast ESIPT, from the acidic to the basic site.[15] Amongst the large range of systems undergoing ESIPT, compounds such as benzoxazoles and naphthoxazoles form an important class.[16] There are reports describing the dependence of fluorescence on solvent polarity[17,20] as well as computations regarding the geometry of the different conformers.[18]

Therefore, taking into consideration the applications and importance of ESIPT inspired molecules and in continuation of our research work on fluorescent materials,[19,20] herein, we report the synthesis of novel ESIPT inspired fluorophore, 2-((4-benzo[*d*]oxazol-2-yl)naphtho[1,2-*d*]oxazol-2-yl)phenol **8** and its photophysical

* Corresponding authors. Tel.: +230 403 7507; fax: +230 465 6928 (P.R.); tel.: +91 22 3361 1111/2707; fax: +91 22 3361 1020 (N.S.); e-mail addresses: ramchemi@intnet.mu (P. Ramasami), n.sekar@ictmumbai.edu.in, nethi.sekar@gmail.com (N. Sekar).
† Tel.: +91 22 3361 1111/2707; fax: +91 22 3361 1020.
‡ Tel.: +230 403 7507; fax: +230 465 6928.

0040-4020/$ – see front matter © 2012 Elsevier Ltd. All rights reserved.
http://dx.doi.org/10.1016/j.tet.2012.11.095

properties and Time-Dependent Density Functional Theory (TD-DFT) explorations.

2. Methodology

2.1. Synthesis strategy

The synthetic scheme for the preparation of 2-((4-benzo[*d*]oxazol-2-yl)naphtho[1,2-*d*]oxazol-2-yl)phenol **8** is shown in Scheme 1. 3-(1,3-Benzoxazol-2-yl)naphthalen-2-ol **3** was prepared by the reported procedure[21] from 3-hydroxynaphthalene-2-carboxylic acid **1** and 2-aminophenol **2** in the presence of PCl_3 in chlorobenzene at 133–135 °C. Sulfanilic acid was diazotized to get 4-sulfobenzenediazonium chloride **5**, which was further coupled with **3** to obtain azo compound **6**. This azo compound **6** was reduced by using sodium dithionate at pH 8–9[22] to get 1-amino-3-(1,3-benzoxazol-2-yl)naphthalene-2-ol **7**, which was confirmed by FTIR, ^{1}H NMR, mass spectral analysis and its M+1 peak was found to be at 277.1. Compound **7**, on treatment with salicylic acid in the presence of phosphorus trichloride in chlorobenzene at reflux temperature (133–135 °C)[21] for 15–18 h gave 2-(4-benzo[*d*]oxazol-2-yl)naphtho[1,2-*d*]oxazol-2-yl)phenol **8**. The synthesized compound **8** was purified by column chromatography and was confirmed by FTIR, ^{1}H NMR, and mass spectral and elemental analyses. Compound **8** showed a distinct stretching vibrational peak for –OH in FTIR at 3352–3367 cm^{-1} and ^{1}H NMR showed the phenolic –OH signal at δ 10.56 ppm and confirmed by D_2O exchange. The phenolic –OH peak disappeared in D_2O exchange with an additional peak appearing at δ 4.80–4.82 ppm. Mass spectral data for compound **8** show M+1 peak at 379.1, which is in good agreement with its molecular weight of M+1 species. Absorption and emission spectra were measured to investigate its photophysical properties and also the solvatochromism and solvatofluorism behaviors of the molecule were studied by measuring electronic absorption and emission spectra in solvents of different polarities.

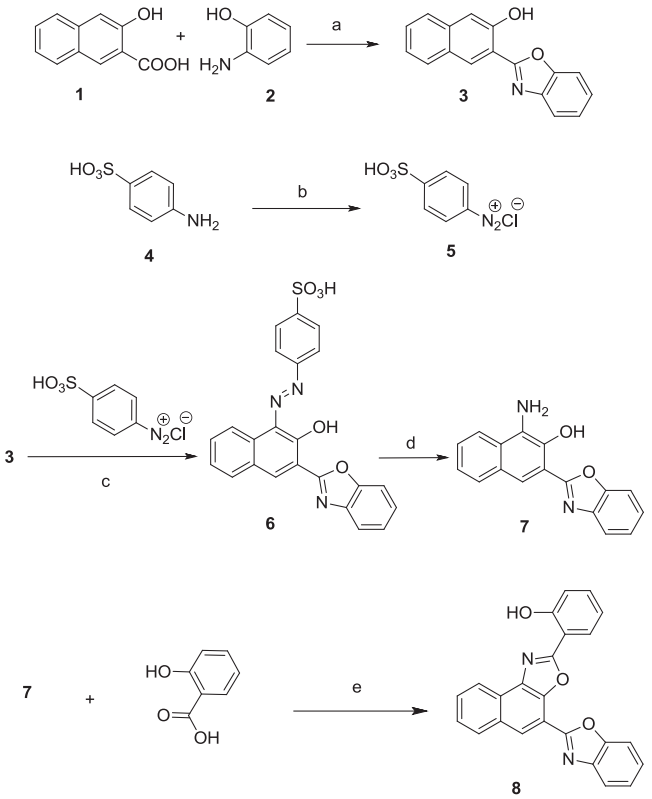

Scheme 1. Synthesis of 2-(4-benzo[*d*]oxazol-2-yl)naphtho[1,2-*d*]oxazol-2-yl)phenol. Reagents and conditions: (a) PCl_3, chlorobenzene, reflux (133–135 °C), 4 h, 79%; (b) $NaNO_2$, HCl, 0–5 °C, 45 min, 98%; (c) methanol/water (80:20), pH 8–9, 0–5 °C, 3 h, 90%; (d) $Na_2S_2O_4$, NaOH, H_2O, 90 °C, 1.5 h, 60%; (e) PCl_3, chlorobenzene, reflux (133–135 °C), 15–16 h, 58%.

2.2. Computational methods

The different conformers of compound **8** and their tautomers involved are illustrated in Fig. 2 The ground state (S_o) geometry of the conformers and tautomers of compound **8** in their C_s symmetry were optimized using the tight criteria in the gas phase using Density Functional Theory (DFT).[23] The functional used was B3LYP. The B3LYP method combines Becke's three parameter exchange functional (B3)[24] with the nonlocal correlation functional by Lee, Yang, and Parr (LYP).[25] The basis set used for all atoms was 6-31G(d), the latter has been justified in the literature[14b,26a,b] for the current investigation. The vibrational frequencies at the optimized structures were computed using the same method to verify that the optimized structures correspond to local minima on the energy surface.[26c]

The vertical excitation energies at the ground state equilibrium geometries were calculated with TD-DFT.[27] The low-lying first singlet excited state (S_1) of each conformer was relaxed using the TD-DFT to obtain its minimum energy geometry. The difference between the energies of the optimized geometries at the first singlet excited state and the ground state was used in computing the emissions.[28] Frequency computations were also carried out on the optimized geometry of the low-lying vibronically relaxed first excited state of conformers. All the computations in solvents of different polarities were carried out using the Polarizable Continuum Model (PCM).[29] All electronic structure computations were carried out using the Gaussian 09 program.[30]

2.3. Relative quantum yield calculations

The quantum yields of compound **8** in different solvents were calculated by using tinopal and fluorescein as reference standards in different solvents using the comparative method.[31] Absorption and emission characteristics of the standards and for compound **8** in polar as well as non-polar solvents were measured at different concentrations at (2, 4, 6, 8, and 10 ppm level). Emission intensity values were plotted against absorbance values and linear plots were obtained. Gradients were calculated for compound **8** in each solvent and for the standards. All the measurements were done by keeping the parameters constant such as solvent and slit width. Relative quantum yields of synthesized compound **8** in different solvents were calculated by using Eq. 1.[31]

$$\Phi_X = \Phi_{St}\left(\frac{Grad_X}{Grad_{St}}\right)\left(\frac{\eta_X^2}{\eta_{St}^2}\right) \quad (1)$$

where: Φ_X: quantum yield of synthesized compound; Φ_{St}: quantum yield of standard sample; $Grad_X$: gradient of synthesized compound; $Grad_{St}$: gradient of standard sample; η_X: refractive index of solvent used for synthesized compound; η_{St}: refractive index of solvent used for standard sample.

Since the molecule has two emissions, the fluorescence quantum efficiency at each emission was calculated using a standard having similar emission at the respective wavelength (for short wavelength emission tinopal (Φ=0.81 in DMF[32]) and for long wavelength emission fluorescein (Φ=0.91 in methanol[33])) was used.

3. Results and discussion

3.1. ESIPT phenomenon

The synthesized compound **8** contains an acidic –OH group at the 2-position with respect to naphtho[1,2-*d*]oxazole ring. The

location of acidic −OH group and =N− groups is such that there is an existence of the intramolecular hydrogen bonding in the ground state. On excitation, the =N− moiety of phenylnaphtho[1,2-*d*][1,3] oxazole ring becomes strongly basic and −OH becomes strongly acidic as shown by the changes in the Mulliken charge distribution in ground and excited states (Supplementary data, Table S4). This leads to the ESIPT, i.e., excited state enol form (K1-Enol*) converts to the excited state keto form (K1-Keto*) (Fig. 1). Absorption of radiation leads to the excitation of the ground state enol (K1-Enol) and it goes to the excited enol (K1-Enol*). This K1-Enol* form either undergoes ESIPT to form the excited state keto form (K1-Keto*) or emits a radiation and returns to the ground state enol form (K1-Enol). The excited state keto form (K1-Keto*) emits radiation and comes to the ground state keto form (K1-Keto). In this way the molecule shows a single absorption around 325 nm (λ_{max}) and dual emission at 411 and 517 nm.

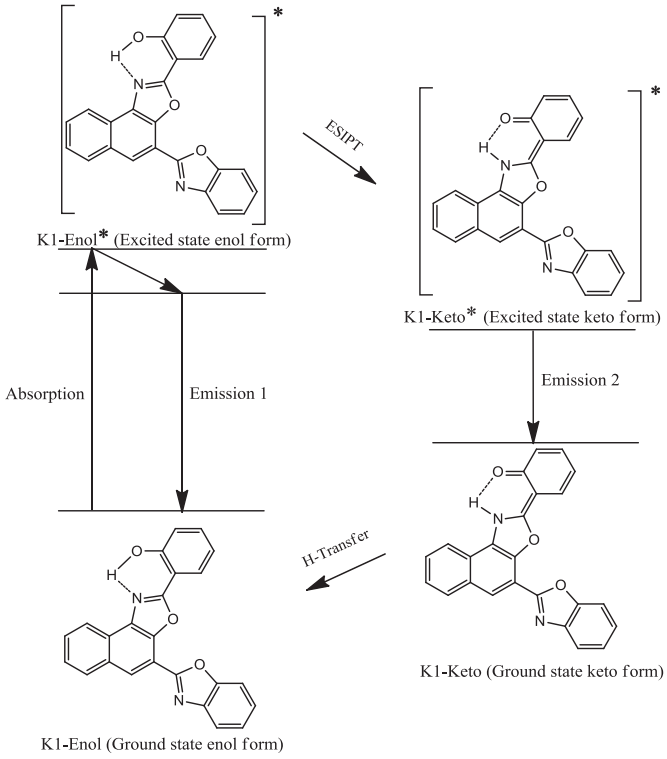

Fig. 1. Excited State Intramolecular Proton Transfer (ESIPT) pathway.

3.2. Rotamers and conformers and their ground state energy

Compound **8** has a fused oxazole ring (at 1- and 2-position of the naphthalene ring), which is rigid and a free benzoxazole ring at the 3-position of the naphthalene ring that can rotate. The naphthalene-fused oxazole ring has a free phenyl group having the *ortho* hydroxyl group participating in the proton hopping at the excited state.[34] In the ground state the molecule can exist in equilibrium between different conformers arising from rotamerism and their tautomers (Fig. 2). The normal planar *syn* form (denoted as K1-Enol) allows an intramolecular hydrogen bond between the acidic −OH group and the basic nitrogen atom of the naphthoxazole ring. The K1-Enol conformer can undergo proton transfer to form its tautomer (denoted as K1-Keto). The conformer K1-Enol can undergo rotamerization around the appended benzoxazolyl group generating the K2-Enol conformer, which on proton transfer leads to the K2-Keto form. In addition to these two enol forms (K1-Enol and K2-Enol), the two other possibilities are the K3-Enol, and the K4-Enol, where the probability of proton transfer happens to be very remote. Compound **8** can coexist in various conformers with their tautomers in solution. DFT computations showed that in all solvents, the keto form is less stable than the enol form, which is preferred in the ground state (Supplementary data, Table S1 and Fig. S1). Among the four enol forms, K1-Enol is the most stable one. The K1-Enol and K2-Enol forms are more stable in polar solvents than in non-polar solvents due to solvation. All the keto forms are prohibitively higher in energy such that they do not exist. The absence of a carbonyl stretching frequency in FTIR (Supplementary data, Fig. S19) indicates that keto is not the preferred configuration in the ground state. The absence of long wavelength absorption is also indicative of the non-existence of the keto form as the absorptive species.

3.3. Absorption and solvatochromism study

Compound **8**, which exists exclusively as the K1-Enol form showed a prominent and intense absorption in all solvents of different polarities, accompanied by two more weak shoulder-like less intense absorptions. The experimental values of absorption maxima together with the molar absorptivity and the vertical excitation values (computed absorption) obtained from the TD-DFT computation are summarized in Table 1. It has been observed that there is close agreement between the experimental λ_{max} and computed vertical excitations.

The largest difference in wavelength between the computed and experimental absorption maxima was 16 nm in acetonitrile for shorter wavelength region. In the case of the long wavelength region it was 10 nm in THF as well as in 1,4-dioxane. In all solvents, the prominent intense absorption can be assigned to HOMO−1 to LUMO transition and the other less intense absorption arises from HOMO−LUMO transition. The frontier molecular orbital (FMO) 98 is HOMO and FMO 99 is LUMO in all cases (Supplementary data, Table S5). It is also observed that the appended benzoxazolyl ring acts as an acceptor; HOMO−LUMO transition is accompanied by the transfer of electrons toward the pending benzoxazolyl ring. It is observed that the electron density is distributed on the naphthoxazole and 2-hydroxy phenyl ring in HOMO. On excitation to the LUMO with a contribution of 67%, the electron density is redistributed equally on all the three ring systems (naphthoxazole, benzoxazole, and 2-hydroxy phenyl ring), which all are in one plane. As an example, in the case of non-polar solvent like chloroform HOMO→LUMO (67%) transition is responsible for vertical excitation located at 378 nm with oscillator strength (*f*) 0.3978 (Fig. 6a), which corresponds to the experimentally observed absorption (shoulder peak) at 373 nm. The HOMO−1 to LUMO (65%) (Supplementary data, Table S5) transition is responsible for the vertical excitation at 336 nm with oscillator strength (*f*) 0.6865, which corresponds to the experimentally observed prominent absorption peak at 325 nm. For polar solvents like DMF, HOMO→LUMO (67%) transition is responsible for vertical excitation located at 377 nm with oscillator strength (*f*) 0.4066 (Fig. 6b), which corresponds to the experimentally observed absorption (shoulder peak) at 379 nm. The HOMO−1 to LUMO (65%) (Supplementary data, Table S5) transition is responsible for the vertical excitation at 336 nm with oscillator strength (*f*) 0.6635, which corresponds to the experimentally observed prominent absorption peak at 325 nm (Table 1 and Fig. 3).

A similar trend is observed in all other solvents (Supplementary data, Figs. S7–S15). This confirms that the experimentally observed short wavelength absorption in the range 320–325 nm is due to the HOMO−1 to LUMO transition and the shoulder peak observed at long wavelength in the range 370–375 nm is due to the HOMO to LUMO transition (Supplementary data, Table S5). The solvatochromism study reveals that the absorption wavelength is

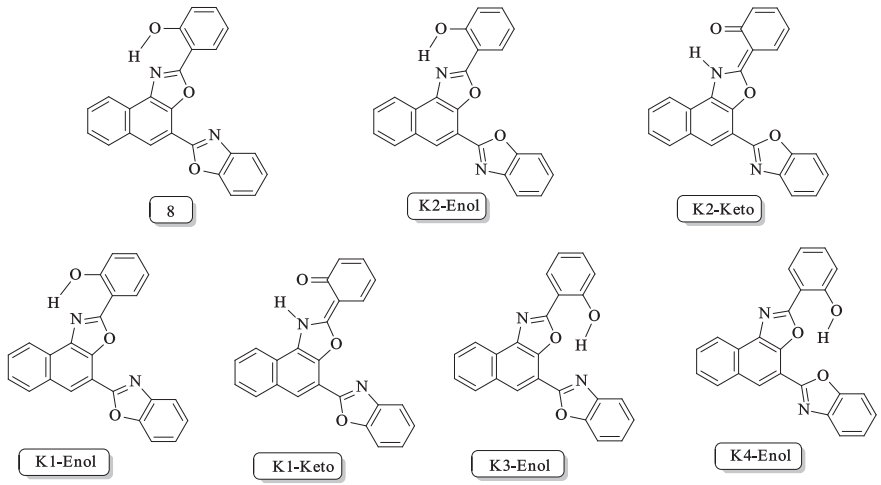

Fig. 2. Conformers and tautomers of compound **8**.

Table 1
Observed UV–visible absorption and computed absorption of compound **8** in different solvents[a]

Solvent	Experimental[b]		TD-DFT[c]			
	λ_{max}^{Expt} (nm)	Molar absorptivity (a) L mol^{-1} cm^{-1}	Vertical excitation		f	Assignment[f]
			nm	eV		
MeOH	322[d]	12,814	335	3.69	0.6279	HOMO−1→LUMO (65%)
	370[e]	5746	376	3.29	0.3825	HOMO→LUMO (67%)
EtOH	322[d]	11,680	336	3.69	0.6412	HOMO−1→LUMO (65%)
	370[e]	5557	376	3.29	0.3897	HOMO→LUMO (67%)
ACN	319[d]	11,831	335	3.69	0.6334	HOMO-1→LUMO (65%)
	370[e]	5746	376	3.29	0.3865	HOMO→LUMO (67%)
DMF	325[d]	18,673	336	3.68	0.6635	HOMO−1→LUMO (65%)
	379[e]	9374	377	3.28	0.4066	HOMO→LUMO (67%)
DCM	325[d]	21,206	336	3.68	0.6710	HOMO−1→LUMO (65%)
	376[e]	10,622	377	3.28	0.3993	HOMO→LUMO (67%)
$CHCl_3$	325[d]	11,264	336	3.68	0.6865	HOMO−1→LUMO (65%)
	373[e]	5746	378	3.27	0.3978	HOMO→LUMO (67%)
EtOAc	322[d]	11,794	336	3.69	0.6582	HOMO−1→LUMO (65%)
	370[e]	6010	377	3.28	0.3842	HOMO→LUMO (67%)
THF	322[d]	11,642	336	3.68	0.6667	HOMO−1→LUMO (65%)
	370[e]	6199	377	3.28	0.3936	HOMO→LUMO (67%)
Dioxane	325[d]	17,955	336	3.68	0.6904	HOMO−1→LUMO (65%)
	370[e]	9526	377	3.26	0.3806	HOMO→LUMO (67%)

[a] Analyses were carried out at room temperature (25 °C).
[b] Experimentally observed λ_{max}.
[c] TD-DFT computations were carried out with the use of optimized structures at B3LYP method with 6-31G(d) basis set.
[d] λ_{max}.
[e] Shoulder peak.
[f] Only major contributions are presented; f=oscillator strength.

insensitive to solvent polarity. However, the absorption intensity is very sensitive to the solvent polarity. The intensity (both computed and observed) of short wavelength absorption is always nearly twice the intensity of long wavelength absorption. The decreasing order of absorption intensity in the short wavelength region is DCM>DMF>1,4-dioxane>MeOH>ACN>EtOAc>EtOH>THF>$CHCl_3$ and in case of long wavelength the order is DMF>1,4-dioxane, THF>EtOAc>$CHCl_3$=ACN=MeOH=EtOH (Table 1, Fig. 3) The excitation spectra mentioned in Fig. 3b were obtained by using shorter (398–436 nm) and longer wavelength (510–544 nm) emissions of the respective solvents.

3.4. Emission and solvatofluorism study

The solvatofluorism study reveals that compound **8** showed dual emission in non-polar solvents (dichloromethane, chloroform, ethyl acetate, THF, and 1,4-dioxane) while in case of the polar solvents (methanol, ethanol, acetonitrile, and *N*,*N*-dimethylformamide) a single emission was observed. It is well known that the long wavelength emission in ESIPT molecules is attributed to the excited state keto tautomer originating from the excited state enol tautomer.[14a] The driving force behind the proton transfer is the associated intrinsic extra stabilization of the keto tautomer at the excited state. This aspect is confirmed by the TD-DFT computations that the excited state keto form has lower energy in non-polar solvents (Table 2) and this reveals that the stabilization is solely intrinsic and not due to the polar environment. The geometry consideration (Section 3.2) favors the keto form in the excited state. TD-DFT computations in the gas phase also reveal that the excited state keto tautomer is more stable (by 9.84 kcal mol^{-1}) and this again confirms that the stability of the keto tautomer in the excited state is intrinsic in nature. The energy considerations are also in favor of a single emission in polar environment. The TD-DFT calculation reveals that there is hardly any difference between the energy of

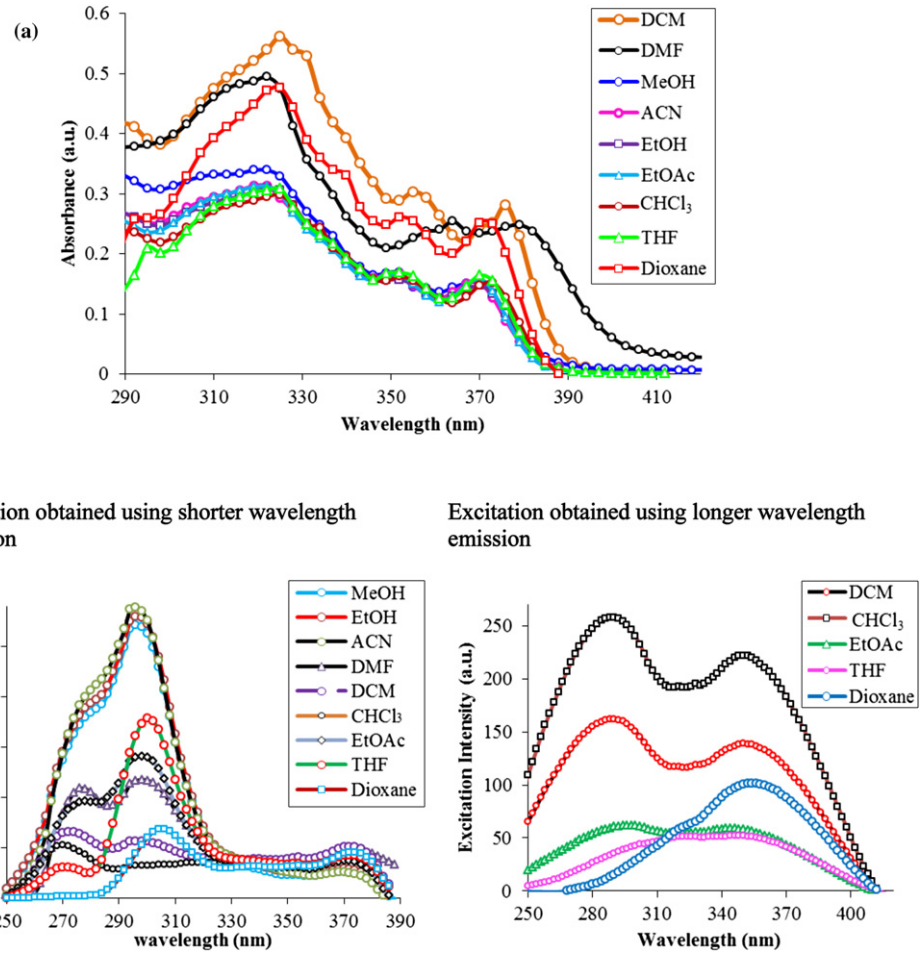

Fig. 3. (a) Absorption spectra of compound **8** in different solvents. (b) Excitation spectra of compound **8** in different solvents.

Table 2
Excited state energy difference between K1-Enol* and K1-Keto* in kcal mol^{-1}[a]

Solvent	MeOH	EtOH	ACN	DMF	DCM	$CHCl_3$	EtOAc	THF	Dioxane
$E'_{Enol} - E'_{Keto}$(kcal mol^{-1})	1.21	1.34	1.18	1.16	2.29	3.53	2.99	2.58	6.03

[a] Excited state energy were computed using TD-DFT with B3LYP method and 6-31G(d) basis set.

optimized enol and keto tautomers at the excited state. The difference between the energies of the optimized geometries at the first singlet excited state and the ground state gives emissions for all the solvents (Supplementary data, Tables S6 and S7).

Quantum yield is sensitive to the solvent polarity (Supplementary data, Fig. S4). It is observed that the quantum yield is higher in non-polar solvents than in polar solvents and this can be attributed to the contribution coming from the long wavelength emission. The quantum efficiency was much higher in DMF (Φ=0.117) than in any other polar solvent. In DMF, compound **8** shows red shift in emission spectra attributed to the deprotonation of −OH group because of the higher basicity of DMF than any other polar solvent. Therefore −H will not be available for the ESIPT (Fig. 3) and hence shows single emission. Similarly, compound **8** has the exceptionally higher quantum yield in chlorinated hydrocarbon solvents (chloroform and DCM) than in oxygenated solvents (ethyl acetate, 1,4-dioxane, and THF; Table 3 and Fig. 5). The short wavelength emission occurs in all cases with a narrow range of Stokes shift (75–79 nm) except in DMF (111 nm). It is interesting to note that the short wavelength emission is much red shifted in DMF (Fig. 4 and Table 3). Solvent polarity does not affect the Stokes shift for shorter emission but longer emission considerably decreases as solvent polarity increases (Supplementary data, Fig. S5).

The cyclic four level photophysical process involving excited state proton transfer (K1-Enol→K1-Enol*→K1-Keto*→K1-Keto) is exemplified in Fig. 6a and b for chloroform and DMF, respectively.

3.5. Structural properties of compound 8

The enol form on photoexcitation at the first excited singlet state undergoes redistribution of charge densities leading to a different geometry in terms of bond angle and bond distance favoring a proton transfer and ultimately the excited state keto form, which becomes an emissive species. This aspect is evident from the TD-DFT computations. The N1–H13, O3–H13, O3–C16, C11–C15 bond distances and Mulliken charges on N1, H13, and O3 of the ground and excited state optimized geometries of the enol form as well as the excited state geometry of keto form are given in Supplementary data, Tables S2–S4, respectively. As a representative example, structural views of the molecule (ground and excited state enol as well as keto forms) in chloroform using Gaussian compatible CYLview software[35] are presented in Fig. 7.

Table 3
Observed and computed emission of compound **8** in various solvents along with its quantum yield and excitation values[a]

Solvent	Experimental (short emission)			TD-DFT (short emission)[c] (nm)	Excitation (nm) (shorter emission)	Experimental (long emission)			TD-DFT (long emission)[c] (nm)	Excitation (nm) (longer emission)	Total quantum yield[e]
	Observed emission (nm)	Stokes shift $\Delta\lambda$ (nm)	Φ^b			Observed emission (nm)	Stokes shift $\Delta\lambda$ (nm)	Φ^d			
MeOH	401	79	0.079	411	296	—	—	—	—	—	0.079
EtOH	400	78	0.077	411	296	—	—	—	—	—	0.077
ACN	398	79	0.063	411	296	—	—	—	—	—	0.063
DMF	436	111	0.117	411	298	—	—	—	—	—	0.117
DCM	400	75	0.175	408	272	514	189	0.238	514	270, 349	0.413
$CHCl_3$	403	78	0.182	406	270	504	179	0.252	526	290, 350	0.434
EtOAc	400	78	0.102	407	298	512	190	0.067	521	296, 344	0.169
THF	400	78	0.135	408	300	520	198	0.131	510	347	0.266
Dioxane	400	75	0.146	401	306	525	200	0.138	544	354	0.284

[a] Analyses were carried out at room temperature (25 °C).
[b] For short wavelength emission, tinopal was used as reference standard.
[c] Computed using TD-DFT method with the B3LYP/6-31G(d).
[d] For long wavelength, fluorescein was used as reference standard.
[e] Summation of short wavelength and long wavelength quantum yield.[19b]

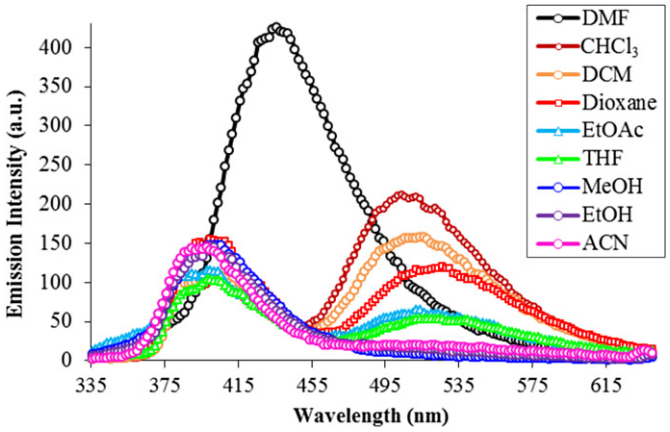

Fig. 4. Emission spectra of compound **8** in various solvents.

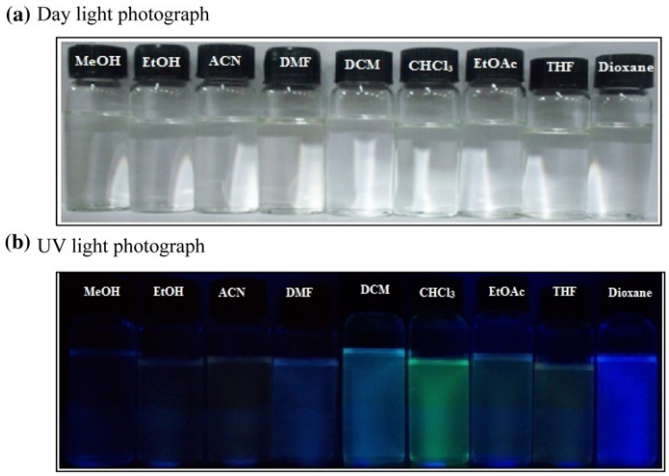

Fig. 5. Day light and UV light photographs of compound **8** in various solvents.

Molecular planarity is the major factor necessary for ESIPT facilitating the proton transfer in the excited state from O3 to N1. In the case of chloroform N1—H13 hydrogen bonding distance decreases by 0.019 Å from K1-Enol (1.802 Å) to K1-Enol* (1.783 Å) while the charge on H13 and O3 was increased by 0.002|e| and 0.009|e| from K1-Enol to K1-Enol*, respectively. The N···H hydrogen bonding distance in HBO is 1.815 Å, which is found to be slightly longer than the K1-Enol ground state.[34] The O3—H13 bond distance increases by 0.006 Å form K1-Enol (0.990 Å) to K1-Enol* (0.996 Å) as reported in Supplementary data, Table S2, which means that in excited state (K1-Enol*) the H13 approaches near to the N1 via hydrogen bonding for transfer of proton (ESIPT). The bond distance C11—C15 decreases from K1-Enol (1.446 Å) to K1-Enol* (1.419 Å) by 0.027 Å while O3—C16 bond distance decreases by 0.015 Å from K1-Enol (1.350 Å) to K1-Enol* (1.335 Å), which is further decreased by 0.074 Å in case of K1-Keto* (1.261 Å) (Supplementary data, Table S3). In addition to this, the bond angle H13—O3—C16 increases by 0.6° from K1-Enol (108.8°) to K1-Enol* (109.4°). In this way, H13 is approaches nearer to N1 in K1-Enol* and further transfer to N1 leads to K1-Keto* with N1—H13 bond distance 1.023 Å and O3—H13 hydrogen bonding distance of 1.934 Å. The K1-Keto* returns to ground state K1-Keto conformer with N1—H13 bond distance of 1.051 Å and O3—H13 hydrogen bonding distance of 1.680 Å (Supplementary data, Table S2). As H13 approaches to O3 the K1-Keto* hydrogen bonding distance decreases by 0.254 Å from 1.934 to 1.680 Å (Supplementary data, Table S2) and it immediately converts to the K1-Keto conformer and then to the K1-Enol. In all the other solvents the N1—H13 hydrogen bond distance is shorter in K1-Enol* than that of the K1-Enol conformer while the O3—H13 hydrogen bond distance is lower in ground state than that of excited state (Fig. 8a and b).

In the case of K1-Enol*, as the solvent polarity increases the N1—H13 hydrogen bonding distance increases from 1.772 to 1.789 Å (Supplementary data, Table S2, Fig. 8a), O3—H13 bond length decreases from 0.998 to 0.995 Å in case of K1-Enol* (Supplementary data, Table S2, Fig. 8b), and O3—C16 bond length increases from 1.332 to 1.338 Å (Supplementary data, Table S3, Fig. 10a) but bond length C11—C15 decreases from 1.422 to 1.416 Å (Supplementary data, Table S3, Fig. 10b). The Mulliken charges on H and O in all solvent increase from K1-Enol to K1-Enol* (Supplementary data, Table S4, Fig. 9a and b) while they decrease for N atom indicating that in K1-Enol* form, H13 is in close proximity of N atom, which is favorable for ESIPT. Further the charges again decrease for K1-Keto*. From K1-Keto* to K1-Keto Mulliken charges for O and N atom decrease while for the H atom it increases (Supplementary data, Table S4, Fig. 9c and d), which supports for the ESIPT process.

3.6. Effect of solvent polarity on ground and excited state dipole moment

As the solvent polarity increases, dipole moment increases in the case of K1-Enol and K1-Keto in both the ground and excited

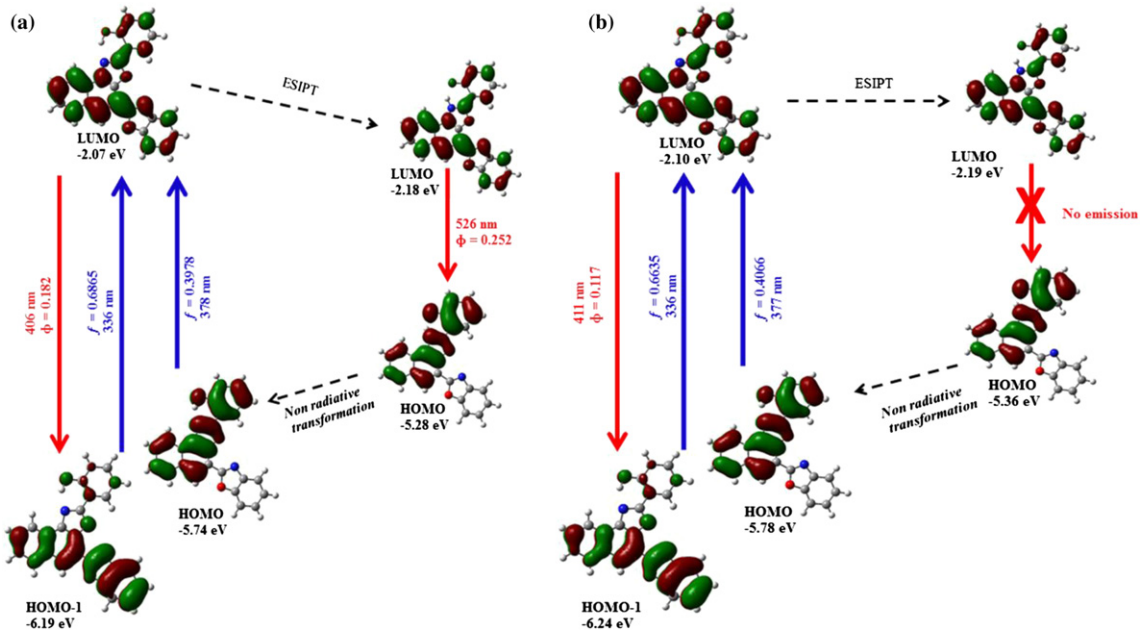

Fig. 6. (a) Representation of the UV–visible absorption and emission of compound **8** in chloroform. The vertical excitation related calculations were based on optimized ground state geometry and the emission based calculations were based on optimized excited state geometry at B3LYP/6-31G(d). The HOMO and LUMO energy levels in the excited state are different from those in the ground state. The FMO involved in the vertical excitation (UV–visible absorption: two blue lines and emission: two red lines). (b) Representation of the UV–visible absorption and emission of compound **8** in DMF. The vertical excitation related calculations were based on optimized ground state geometry and the emission based calculations were based on optimized excited state geometry at B3LYP/6-31G(d). The HOMO and LUMO energy levels in the excited state are different from those in the ground state. The FMO involved in the vertical excitation (UV–visible absorption: two blue lines and emission: one red line).

states. The ratio of dipole moment in excited to ground state in different solvents is plotted against the solvent function (E_T^N) (Table 4, Fig. 11a and b). The solvent polarity function has been taken from the literature.[36] The calculated dipole moment ratio for shorter emission is 1.101 and is 2.231 for longer emission. K1-Keto shows the highest dipole moment in both the states, in the excited state it ranges from 8.044 to 9.899 D while in the ground state it ranges from 5.531 to 8.255 D. K1-Enol shows the lower dipole moment in both the states, in the excited state it ranges from 2.726 to 3.259 D and in the ground state it ranges from 2.802 to 3.817 D.

4. Conclusion

To conclude, this paper reports the synthesis of the fluorescent 2-((4-benzo[*d*]oxazol-2-yl)naphtho[1,2-*d*]oxazol-2-yl)phenol. This compound is well characterized by ^{1}H NMR, ^{13}C NMR, and mass spectroscopy. It shows a single prominent absorption and emission in solvents, single emission in polar solvents, and dual emission in non-polar solvents. The highest quantum efficiency was observed in chloroform (Φ=0.434). The absorption and emission wavelengths were computed using TD-DFT and they are in good agreement with the experimental results. To the best of our knowledge, only a few naphthalene-based ESIPT molecules are described in the literature and this report is the first one that uses the computational chemistry to gain further insight into the ESIPT process at the molecular level.

5. Experimental section

5.1. General

All commercial reagents were purchased and used without purification and all solvents were reagent grade. The reaction was monitored by TLC using on 0.25 mm silica gel 60 F_{254} precoated plates, which were visualized with UV light. Melting points were measured on standard melting point apparatus and are uncorrected. The FTIR spectra were recorded on a Fourier Transform IR instrument (ATR accessories). ^{1}H NMR and ^{13}C NMR spectra were recorded on Varian Cary Eclipse, MR-300 MHz, USA, NMR spectrometer operating at 300 and 75 MHz, respectively, using TMS as an internal standard. Mass spectra were recorded on Finnigan Mass Spectrometer instrument. The absorption spectra of the compounds were recorded on a Spectronic Genesys 2 UV–visible spectrophotometer; fluorescence emission spectra were recorded on Varian Cary Eclipse fluorescence spectrophotometer using freshly prepared solutions. Quantum yields were calculated by using tinopal (Φ=0.81 in DMF[32]) for shorter emission and fluorescein (Φ=0.91 in methanol[33]) for longer emission as reference standards.

5.2. Experimental procedure

*5.2.1. 3-(1,3-Benzoxazol-2-yl)naphthalen-2-ol (**3**).* A mixture of 2-aminophenol **2** (1.09 g, 0.01 mol) and 3-hydroxynaphthalene-2-carboxylic acid **1** (1.88 g, 0.01 mol) was refluxed (133–135 °C) in chlorobenzene (10 mL) in the presence of PCl_3[21] (2 g, 1.3 mL, 0.01 mol) for 4 h. After completion of reaction, the solid product was precipitated out and was filtered to give crude product **3**. Yield 2.06 g (79%), which was further recrystallized from ethanol, mp: 171–173 °C (lit. mp: 171–172 °C[21b]).

*5.2.2. 4-{[3-(1,3-Benzoxazol-2-yl)-2-hydroxynaphthalen-1-yl]diazenyl}benzenesulfonic acid (**6**).* Sulfanilic acid **4** (2.07 g, 0.012 mol) was dissolved in water (10 mL) containing sodium carbonate of (0.62 g) at 50–55 °C. A solution of $NaNO_2$ (0.84 g, 0.012 mol) in water (10 mL) was added to sulfanilic acid solution in water and then this mixture was added slowly to the concd HCl (4 mL) at 0–5 °C for 30 min and further stirred at this temperature for 1.5 h to get 4-sulfobenzenediazonium chloride salt **5**. This was further coupled with the 3-(1,3-benzoxazol-2-yl)naphthalene-2-ol **3**

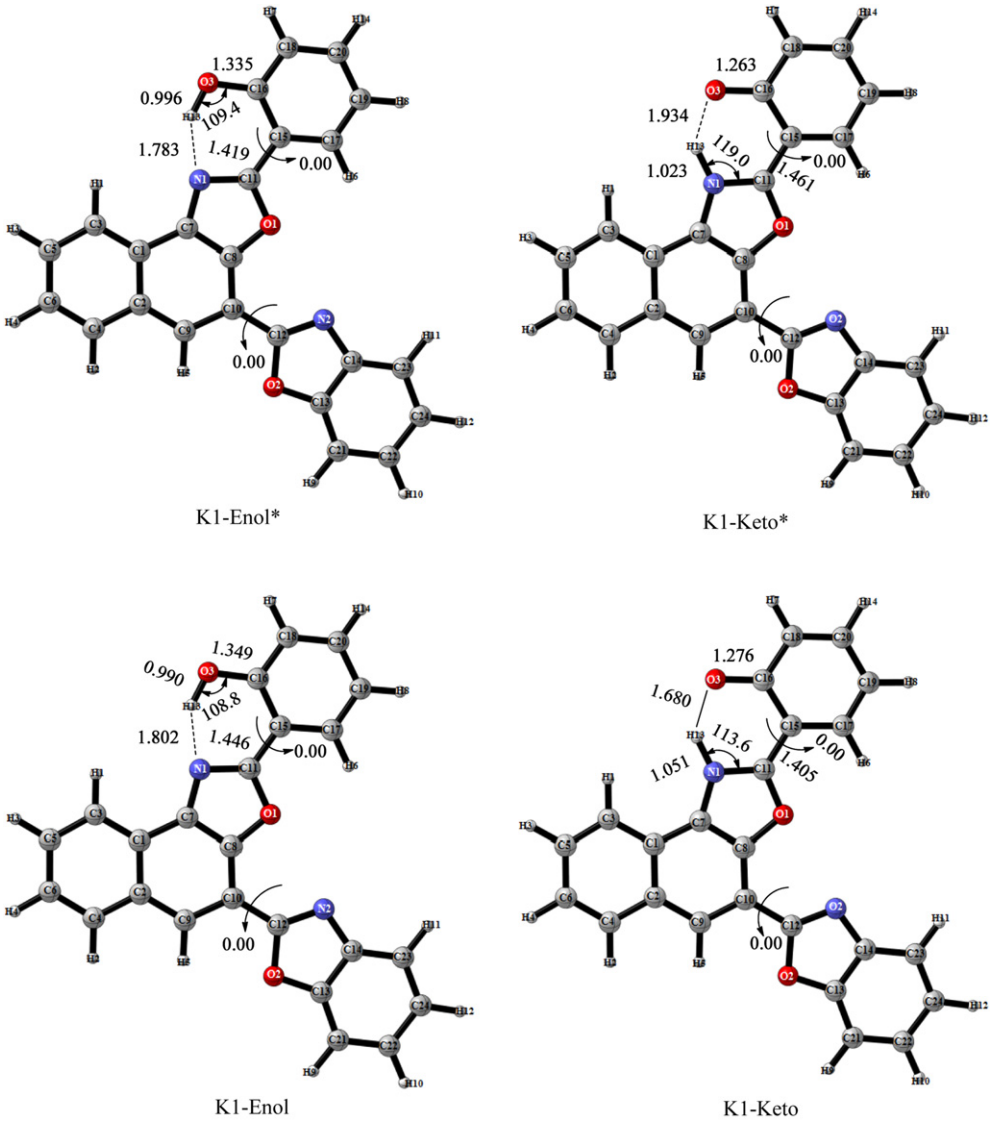

Fig. 7. Ground and excited state optimized structural conformations of compound **8** in chloroform. These figures were obtained from Gaussian compatible CYLview software.[35]

(2.61 g, 0.010 mol) at 0–5 °C at pH 8–9 for 3 h and then at room temperature for 1 h in methanol/water mixture (80:20). Then reaction mixture was neutralized with acetic acid (9–10 mL) at pH 7, methanol was removed under reduced pressure and then filtered out to afford 4-{[3-(1,3-benzoxazol-2-yl)-2-hydroxynaphthalen-1-yl]diazenyl}benzenesulfonic acid **6**. Yield 4.0 g, (90%). Recrystallized from ethyl alcohol, mp: 234 °C.

*5.2.3. 1-Amino-3-(1,3-benzoxazol-2-yl)naphthalen-2-ol (**7**).* The azo compound **6** (4.45 g, 0.010 mol) was heated in water containing

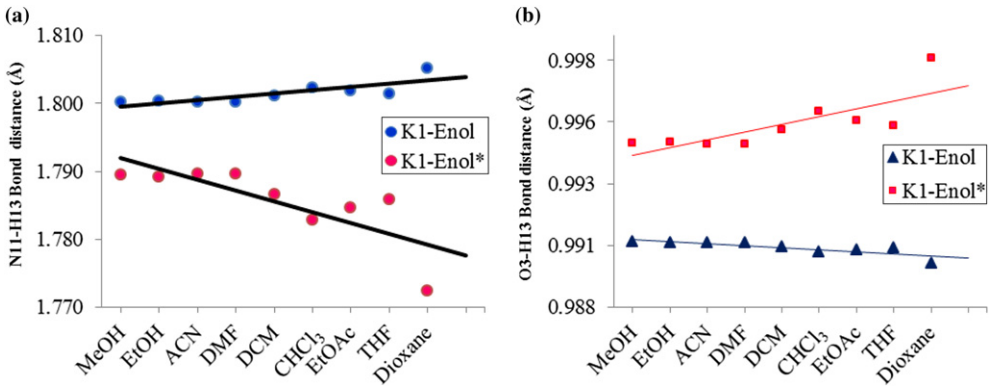

Fig. 8. Plot of N1–H13 and O3–H13 bond distances in K1-Enol against solvents.

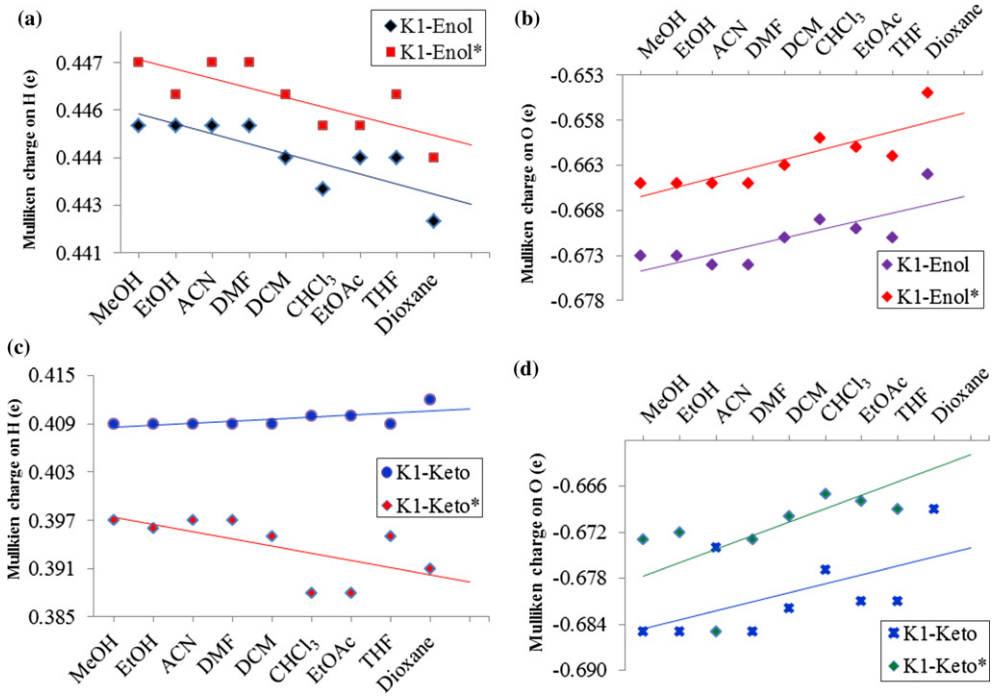

Fig. 9. Plot of Mulliken charges on H, N, and O atoms of K1-Enol in ground and excited states.

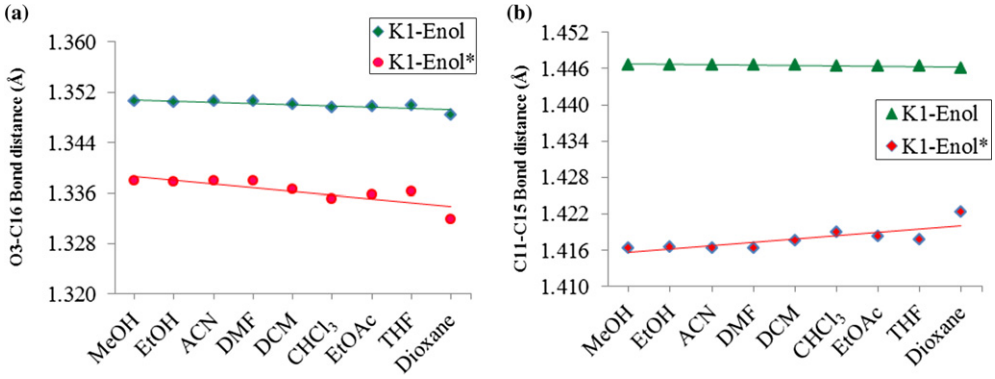

Fig. 10. Plot of O3–C16 and C11–C15 bond distance in K1-Enol and K1-Enol* versus solvents.

Table 4
Dipole moment (μ in Debye) of K1-Enol in ground state and excited state in various solvents

Medium	E_T^N	μ_g K1-Enol[a]	μ_e K1-Enol*[b]	$\frac{\mu_e \text{ Enol}}{\mu_g \text{ Enol}}$	μ_g K1-Keto[a]	μ_e K1-Keto*[b]	$\frac{\mu_e \text{ Keto}}{\mu_g \text{ Keto}}$	Experimental
MeOH	0.775	3.810	3.254	0.854	8.237	9.891	1.201	1.101 (Short wavelength emission)
EtOH	0.654	3.791	3.240	0.855	8.190	9.870	1.205	2.231 (Long wavelength emission)
ACN	0.460	3.815	3.258	0.854	8.250	9.896	1.200	
DMF	0.386	3.817	3.259	0.854	8.255	9.899	1.199	
DCM	0.309	3.775	3.229	0.855	8.250	9.850	1.194	
$CHCl_3$	0.259	3.663	3.259	0.890	7.866	9.712	1.235	
EtOAc	0.228	3.509	3.051	0.869	7.470	8.044	1.077	
THF	0.207	3.575	3.093	0.865	7.641	8.044	1.053	
Dioxane	0.164	3.626	3.126	0.862	7.771	9.662	1.243	

[a] Dipole moments were obtained at the optimized ground state geometry.
[b] Dipole moments were obtained at the optimized excited state geometry.

NaOH (3.51 g, 0.088 mol) at 50 °C and sodium dithionate (3.78 g, 0.025 mol) was added at 90 °C in portions over period of 1 h. The mixture was heated at 90 °C at pH 8–9 until the color of azo disappeared (1.5 h).[21] The progress of the reaction was monitored by TLC. After completion of reaction, the reaction mass was neutralized up to pH 7, filtered and washed well with water 2–3 times, and dried well to afford crude 1-amino-3-(1,3-benzoxazol-2-yl)naphthalen-2-ol **7**. Yield 1.65 g (60%). Crude product was recrystallized in ethyl alcohol, mp: 206–208 °C.

*5.2.4. 2-((4-Benzo[d]oxazol-2-yl)naphtho[1,2-d]oxazol-2-yl)phenol (**8**).* 1-Amino-3-(1,3-benzoxazol-2-yl) naphthalen-2-ol **7** (0.010 mol),

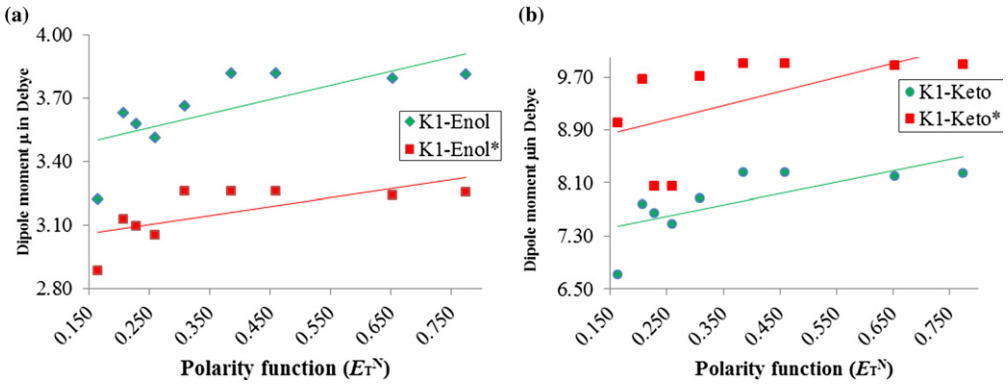

Fig. 11. Plots of dipole moment (μ) versus solvent polarity function (E_T^N).

2-hydroxybenzoic acid (0.010 mol), and PCl_3[21] (0.015 mol) were refluxed in chlorobenzene (130–133 °C) (6 mL) until completion of reaction (16–18 h) and was confirmed by TLC. After cooling the reaction mass, solid product was filtered out and recrystallized from chloroform to afford corresponding compound **8**. Yield 2.19 g (58%), which was purified by column chromatography using hexane/ethyl acetate mixture as eluant (8:2), mp: 208–210 °C.

5.3. Spectral data of compounds 7 and 8

*5.3.1. 1-Amino-3-(1,3-benzoxazol-2-yl)naphthalen-2-ol (**7**).* FTIR 3510, 3452, 3357 ($\nu_{N-H,\ O-H}$), 3028 ($\nu_{Aromatic\ C-H\ Stretching}$), 1615, 1585, 1477 ($\nu_{C=C,\ C=N\ ring\ stretching}$), 1222, 1132 ($\nu_{C-O\ stretching}$), 750 ($\nu_{Aromatic\ C-H\ out\ of\ plane\ bending}$) cm^{-1}.

^1H NMR (DMSO-d_6 300 MHz) δ=6.85 (d, J=7.9 Hz, 1H, Ar–H), 7.36–7.43 (m, J=7.8, 8.2, 1.8 Hz, 5H, Ar–H), 7.48 (dd, J=8.2, 1.9 Hz, 1H, Ar–H), 7.92 (dd, J=8.5, 1.6 Hz, 1H, Ar–H), 8.73 (s, 1H, Ar–H), 9.96 (s, 2H, -NH_2), 10.12 (s, 1H, -OH) ppm.

^{13}C NMR (DMSO-d_6 75 MHz) δ=111.5, 113.3, 119.9, 124.6, 125.9, 126.7, 127.2, 127.5, 129.2, 136.6, 145.9, 149.5, 153.9, 162.4.

MS (m/z) 277.1 (M+1, 99%), 276.1 (75%), 275 (30%), 246.1 (18%), 124.1 (20%).

Anal. Calcd for $C_{17}H_{12}N_2O_2$: C, 73.90; H, 4.38; N, 10.14. Found: C, 73.87; H, 4.21; N, 10.03.

*5.3.2. 2-((4-Benzo[d]oxazol-2-yl)naphtho[1,2-d]oxazol-2-yl)phenol (**8**).* FTIR 3367 ($\nu_{O-H\ stretching}$), 3050 ($\nu_{Aromatic\ C-H\ stretching}$), 1636, 1581, 1537 ($\nu_{C=C,\ C=N\ ring\ stretching}$), 1243, 1209, 1168 ($\nu_{C-O\ stretching}$), 733 ($\nu_{Aromatic\ -CH\ out\ of\ plane\ bending\ vibration}$) cm^{-1}.

^1H NMR ($CDCl_3$, 300 MHz) δ=6.92 (dd, J=7.8, 7.2 Hz, 1H, Ar–H), 7.02 (d, J=8.4 Hz, 1H, Ar–H), 7.10 (dd, J=10.8, 8.1 Hz, 1H, Ar–H), 7.18 (d, J=7.8 Hz, 1H, Ar–H), 7.45–7.52 (m, J=7.5, 2.7, 1.8 Hz, 2H, Ar–H), 7.62 (dd, J=7.2, 1.8 Hz, 1H, Ar–H), 7.75 (m, J=7.2, 1.5 1H, Ar–H), 7.92 (m, J=8.1, 1.5, 1.8 Hz, 1H, Ar–H), 8.10 (d, J=8.1 Hz, 1H, Ar–H), 8.32 (dd, J=8.1, 1.5 Hz, 1H, Ar–H), 8.50 (d, J=8.2 Hz, 1H, Ar–H), 8.74 (s, 1H, Ar–H), 10.55 (s, 1H, Ar–OH) ppm.

^1H NMR (D_2O exchange) ($CDCl_3$, 300 MHz) δ=4.82 (s, 1H, H–OD), 6.92 (dd, J=7.8, 7.2 Hz, 1H, Ar–H), 7.0 (d, J=8.4 Hz, 1H, Ar–H), 7.11 (dd, J=10.8, 8.1 Hz, 1H, Ar–H), 7.18 (d, J=7.8 Hz, 1H, Ar–H), 7.45–7.52 (m, J=7.5, 2.7, 1.8 Hz, 2H, Ar–H), 7.62 (dd, J=7.2, 1.8 Hz, 1H, Ar–H), 7.75 (m, J=7.2, 1.5 1H, Ar–H), 7.92 (m, J=8.1, 1.5, 1.8 Hz, 1H, Ar–H), 8.11 (d, J=8.1 Hz, 1H, Ar–H), 8.32 (dd, J=8.1, 1.5 Hz, 1H, Ar–H), 8.50 (d, J=8.2 Hz, 1H, Ar–H), 8.74 (s, 1H, Ar–H) ppm.

^{13}C NMR (DMSO-d_6, 75 MHz) δ=111.4 (strong), 112.1, 113.0, 119.8 (strong), 123.0, 125.4, 125.7, 126.3, 126.5, 127.1, 123.3, 128.2, 129.7, 130.3, 130.9, 136.4, 140.1, 142.6, 144.1, 149.5, 154.4, 162.3 ppm.

MS (m/z): 379.1 (M+1, 100%), 380.1 (25%).

Anal. Calcd for $C_{24}H_{14}N_2O_3$: C, 76.18; H, 3.73; N, 7.40. Found: C, 76.03; H, 3.55; N, 7.23.

Acknowledgements

K.P. is thankful to UGC-CAS for providing research fellowship under Special Assistance Programme (SAP). N.S. and V.G. are thankful to the 5th UGC-TEC Consortium agreement for financial support. A.T. is grateful to UGC for research support under Major Research Project as well as UGC-CSIR fellowship. V.P. is thankful for postdoctoral fellowship from the Principal Scientific Adviser (PSA), Govt. of India. The authors acknowledge the useful comments from anonymous reviewers and the editor to improve the manuscript.

Supplementary data

Supplementary data associated with this article can be found in the online version, at http://dx.doi.org/10.1016/j.tet.2012.11.095.

References and notes

1. (a) Abou-Zied, O. K.; Jimenez, R.; Romesberg, F. E. *J. Am. Chem. Soc.* **2001**, *123*, 4613–4614; (b) Ogawa, A. K.; Abou-Zied, O. K.; Tsui, V.; Jimenez, R.; Case, D. A.; Romesberg, F. E. *J. Am. Chem. Soc.* **2000**, *122*, 9917–9920.
2. (a) Yu, W. S.; Cheng, C. C.; Cheng, Y. M.; Wu, P. C.; Song, Y. H.; Chi, Y.; Chou, P. T. *J. Am. Chem. Soc.* **2003**, *125*, 10800–10801; (b) Chou, P. T.; Huang, C. H.; Pu, S. C.; Cheng, Y. M.; Liu, Y. H.; Wang, Y.; Chen, C. T. *J. Phys. Chem. A* **2004**, *108*, 6452–6454; (c) Rodembusch, F. S.; Campo, L. F.; Stefani, V.; Rigacci, A. *J. Mater. Chem.* **2005**, *15*, 1537–1541; (d) Lim, S. J.; Seo, J.; Soo, Y. P. *J. Am. Chem. Soc.* **2006**, *128*, 14542–14547; (e) Cardoso, M. B.; Samios, D.; Silveira, N. P.; Rodembusch, F. S.; Stefani, V. *Photochem. Photobiol. Sci.* **2007**, *6*, 99–102; (f) Mutai, T.; Tomoda, H.; Ohkawa, T.; Yabe, Y.; Araki, K. *Angew. Chem., Int. Ed.* **2008**, *47*, 9522–9524.
3. Chen, C. L.; Lin, C. W.; Hsieh, C. C.; Lai, C. H.; Lee, G. H.; Wang, C. C.; Chou, P. T. *J. Phys. Chem. A* **2009**, *113*, 205–214.
4. Chen, K. Y.; Hsieh, C. C.; Cheng, Y. M.; Lai, C. H.; Chou, P. T. *Chem. Commun.* **2006**, 4395–4397.
5. Chen, K. Y.; Cheng, Y. M.; Lai, C. H.; Hsu, C. C.; Ho, M. L.; Lee, G. H.; Chou, P. T. *J. Am. Chem. Soc.* **2007**, *129*, 4534–4535.
6. Stephan, J. S.; Rodriguez, C. R.; Grellmann, K. H.; Zachariasse, K. A. *Chem. Phys.* **1994**, *186*, 435–446.
7. Seo, J.; Kim, S.; Park, S. Y. *J. Am. Chem. Soc.* **2004**, *126*, 11154–11155.
8. (a) Chou, P.; McMorrow, D.; Aartsma, T. J.; Kasha, M. *J. Phys. Chem.* **1984**, *88*, 4596–4599; (b) Acuna, A. U.; Amat-Guerri, F.; Costela, A.; Douhal, A.; Figuera, J. M.; Florido, F.; Sastre, R. *Chem. Phys. Lett.* **1991**, *187*, 98–102; (c) Park, S.; Kwon, O. H.; Kim, S.; Park, S.; Choi, M. G.; Cha, M.; Park, S. Y.; Jang, D. J. *J. Am. Chem. Soc.* **2005**, *127*, 10070–10074; (d) Sakai, K.; Ichikawaa, M.; Taniguchi, Y. *Chem. Phys. Lett.* **2006**, *420*, 405–409; (e) Osken, I.; Sahin, O.; Gundogan, A. S.; Bildirir, H.; Capan, A.; Ertas, E.; Eroglu, M. S.; Wallis, J. D.; Topal, K.; Ozturk, T. *Tetrahedron* **2012**, *68*, 1216–1222; (f) Lodeiro, J. F.; Nunez, C.; Carreira, R.; Santos, H. M.; Lopez, C. S.; Mejuto, J. C.; Capelo, J. C.; Lodeiro, C. *Tetrahedron* **2011**, *67*, 326–333.
9. (a) Sytnik, A.; Del Valle, J. C. *J. Phys. Chem* **1995**, *99*, 13028–13032; (b) Dennison, S. M.; Gubaray, J.; Sengupta, P. K. *Spectrochim. Acta, Part A* **1999**, *55*, 1127–1132; (c) Holler, M. G.; Campo, L. F.; Brandelli, A.; Stefani, V. *J. Photochem. Photobiol., A: Chem.* **2002**, *149*, 217–225; (d) Shynkar, V. V.; Klymchenko, A. S.; Kunzelmann, C.; Duportail, G.; Muller, C. D.; Demchenko, A. P.; Freyssinet, J.-M.; Mely, Y. *J. Am. Chem. Soc.* **2007**, *129*, 2187–2193; (e) Kim, T. I.; Kang, H. J.; Han, G.; Chung, S. J.;

Kim, Y. *Chem. Commun.* **2009**, 5895–5897; (f) Xu, Y.; Pang, Y. *Chem. Commun.* **2010**, 4070–4072.
10. (a) Zhang, H.; Han, L. F.; Zachariasse, K. A.; Jiang, Y. B. *Org. Lett.* **2005**, *7*, 4217–4220; (b) Stein, M.; Keck, J.; Waiblinger, F.; Fluegge, A. P.; Kramer, H. E. A.; Hartschuh, A.; Port, H.; Leppard, D.; Rytz, G. *J. Phys. Chem. A* **2002**, *106*, 2055–2066; (d) Helal, A.; Kim, H. S. *Tetrahedron* **2010**, *66*, 7097–7103; (e) Dong, D.; Jing, X.; Zhang, X.; Hu, X.; Wu, Y.; Duan, C. *Tetrahedron* **2012**, *68*, 306–310; (f) Yan, L.; Ye, Z.; Peng, C.; Zhang, S. *Tetrahedron* **2012**, *68*, 2725–2727; (g) Chen, W.; Wright, B. D.; Pang, Y. *Chem. Commun.* **2012**, 3824–3826; (h) Chu, Q.; Medvetz, D. A.; Pang, Y. *Chem. Mater.* **2007**, *19*, 6421–6429; (i) Taki, M.; Wolford, J. L.; O'Halloran, T. V. *J. Am. Chem. Soc.* **2004**, *126*, 712–713; (j) Chen, W. H.; Xing, Y.; Pang, Y. *Org. Lett.* **2011**, *13*, 1362–1365.
11. (a) Sun, W. H.; Li, S. Y.; Hu, R.; Qian, Y.; Wang, S. Q.; Yang, G. Q. *J. Phys. Chem. A* **2009**, *113*, 5888–5895; (b) Park, S.; Kwon, J. E.; Kim, S. H.; Seo, J.; Chung, K.; Park, S.; Jang, D.; Medina, B. M.; Gierschner, J.; Park, S. Y. *J. Am. Chem. Soc.* **2009**, *131*, 14043–14049; (c) Rodriguez, J. G.; Tejedor, J. L. *Tetrahedron* **2005**, *61*, 2047–2054.
12. Chou, P.-T.; Martinez, M. L. *Radiat. Phys. Chem.* **1993**, *41*, 373–378.
13. (a) Kim, S.; Park, S. Y. *Adv. Mater.* **2003**, *15*, 1341–1344; (b) Kim, S.; Park, S. Y.; Tashida, I.; Kawai, H.; Nagamura, T. *J. Phys. Chem. B* **2002**, *106*, 9291–9294.
14. (a) Zhao, J.; Ji, S.; Chen, Y.; Guo, H.; Yang, P. *Phys. Chem. Chem. Phys.* **2012**, *14*, 8803–8817; (b) Kim, C. H.; Park, J.; Seo, J.; Park, S. Y.; Joo, T. *J. Phys. Chem. A* **2010**, *114*, 5618–5629.
15. (a) Formosinho, S. J.; Arnaut, L. G. *J. Photochem. Photobiol., A* **1993**, *75*, 21–48; (b) Kasha, M. *J. Chem. Soc., Faraday Trans. II* **1986**, *82*, 2379–2392.
16. Alfonso, B.; Flor, R.; Manuel, M.; Miguel, A. R.; Carmen, M. *J. Phys. Chem. A* **2009**, *113*, 56–67.
17. Das, K.; Sarkar, N.; Gosh, A. K.; Majumdar, D.; Nath, D. N.; Bhattacharyya, K. *J. Phys. Chem.* **1994**, *98*, 9126–9132.
18. (a) Santra, S.; Dogra, S. K. *Chem. Phys.* **1998**, *226*, 285–296; (b) Fores, M.; Duran, M.; Sola, M.; Orozco, M.; Luque, F. J. *J. Phys. Chem. A* **1999**, *103*, 4525–4532; (c) Premvardhan, L.; Peteanu, L. *Chem. Phys. Lett.* **1998**, *296*, 521–529; (d) Fores, M.; Duran, M.; Sola, M.; Adamowicz, L. *J. Phys. Chem. A* **1999**, *103*, 4413–4420.
19. (a) Padalkar, V. S.; Tathe, A. B.; Gupta, V. D.; Patil, V. S.; Phatangare, K. R.; Sekar, N. *J. Fluoresc.* **2012**, *22*, 311–322; (b) Patil, V. S.; Padalkar, V. S.; Phatangare, K. R.; Gupta, V. D.; Umape, P. G.; Sekar, N. *J. Phys. Chem. A* **2012**, *116*, 536–545.
20. Gupta, V. D.; Padalkar, V. S.; Phatangare, K. R.; Patil, V. S.; Umape, P. G.; Sekar, N. *Dyes Pigments* **2011**, *88*, 378–384.
21. (a) Ueno, R.; Kitayama, Y.; Minami, K.; Wakamori, H. European Patent EP1380564 A1, 2004. (b) Matsui, K.; Kuroda, T. *Kogyo Kagaku Zasshi (The Journal of the Society of Chemical Industry, Japan)* **1967**, *70*, 2325–2329.
22. Rangnekar, D. W.; Rajadhyaksha, D. D. *Dyes Pigments* **1986**, *7*, 365–372.
23. Treutler, O.; Ahlrichs, R. *J. Chem. Phys.* **1995**, *102*, 346–354.
24. Becke, A. D. *J. Chem. Phys.* **1993**, *98*, 1372–1377.
25. Lee, C.; Yang, W.; Parr, R. G. *Phys. Rev. B* **1988**, *37*, 785–789.
26. (a) Casida, M. E.; Jamorski, C.; Salahub, D. R. *J. Chem. Phys.* **1998**, *108*, 4439–4449; (b) Santra, M.; Moon, H.; Park, M.-H.; Lee, T.-W.; Kim, Y. K.; Ahn, K. H. *Chem.—Eur. J.* **2012**, *18*, 9886–9893; (c) Li, H.; Niu, L.; Xu, X.; Zhang, S.; Gao, F. *J. Fluoresc.* **2011**, *21*, 1721–1728.
27. (a) Hehre, W. J.; Radom, L.; Schleyer, P. v. R.; Pople, J. *Ab Initio Molecular Orbital Theory*; Wiley: New York, NY, 1986; (b) Bauernschmitt, R.; Ahlrichs, R. *Chem. Phys. Lett.* **1996**, *256*, 454–464; (c) Furche, F.; Rappaport, D. Density Functional Theory for Excited States: Equilibrium Structure and Electronic Spectra In-*Olivucci, M., Ed.. Computational Photochemistry*; Elsevier: Amsterdam, 2005; Vol. 16, Chapter 3.
28. Lakowicz, J. R. *Principles of Fluorescence Spectroscopy*, 2nd ed.; Kluwer Academic: New York, NY, 1999; (b) Valeur, B. *Molecular Fluorescence: Principles and Applications*; Wiley-VCH: Weinheim, 2001.
29. (a) Cossi, M.; Barone, V.; Cammi, R.; Tomasi, J. *Chem. Phys. Lett.* **1996**, *255*, 327–335; (b) Tomasi, J.; Mennucci, B.; Cammi, R. *Chem. Rev.* **2005**, *105*, 2999–3094.
30. Frisch, M. J.; Trucks, G. W.; Schlegel, H. B.; Scuseria, G. E.; Robb, M. A.; Cheeseman, J. R.; Scalmani, G.; Barone, V.; Mennucci, B.; Petersson, G. A.; Nakatsuji, H.; Caricato, M.; Li, X.; Hratchian, H. P.; Izmaylov, A. F.; Bloino, J.; Zheng, G.; Sonnenberg, J. L.; Hada, M.; Ehara, M.; Toyota, K.; Fukuda, R.; Hasegawa, J.; Ishida, M.; Nakajima, T.; Honda, Y.; Kitao, O.; Nakai, H.; Vreven, T.; Montgomery, J. A., Jr.; Peralta, J. E.; Ogliaro, F.; Bearpark, M.; Heyd, J. J.; Brothers, E.; Kudin, K. N.; Staroverov, V. N.; Kobayashi, R.; Normand, J.; Raghavachari, K.; Rendell, A.; Burant, J. C.; Iyengar, S. S.; Tomasi, J.; Cossi, M.; Rega, N.; Millam, N. J.; Klene, M.; Knox, J. E.; Cross, J. B.; Bakken, V.; Adamo, C.; Jaramillo, J.; Gomperts, R.; Stratmann, R. E.; Yazyev, O.; Austin, A. J.; Cammi, R.; Pomelli, C.; Ochterski, J. W.; Martin, R. L.; Morokuma, K.; Zakrzewski, V. G.; Voth, G. A.; Salvador, P.; Dannenberg, J. J.; Dapprich, S.; Daniels, A. D.; Farkas, O.; Foresman, J. B.; Ortiz, J. V.; Cioslowski, J.; Fox, D. J. *Gaussian 09, Revision C.01*; Gaussian: Wallingford, CT, 2010.
31. (a) Williams, A. T. R.; Winfield, S.; Miller, J. N. *Analyst* **1983**, *108*, 1067–1071; (b) Dhami, S.; De Mello, A. J.; Rumbles, G.; Bishop, S. M.; Phillips, D.; Beeby, A. *Photochem. Photobiol.* **1995**, *61*, 341–346.
32. http://www.mufong.com.tw/Ciba/ciba_guid/optical_brighteners.pdf.
33. Magde, D.; Wong, R.; Seybold, P. G. *Photochem. Photobiol* **2002**, *75*, 327–334.
34. Chen, W.; Twum, E. B.; Li, L.; Wright, B. D.; Rinaldi, P. L.; Pang, Y. *J. Org. Chem.* **2012**, *77*, 285–290.
35. Legault, C. Y. *CYLview, 1.0b*; Université de Sherbrooke: 2009; http://www.cylview.org.
36. Reichardt, C. *Solvent and Solvent Effects in Organic Chemistry Third and Enlarged Edition*; Wiley VCH: Weinheim, Germany, 2003.